Article citation info:
Fisli Y, Rezaiguia A, Guenfoud S, Laefer DF. Dynamic response of a multi-span, orthotropic bridge deck under moving truck loading with tandem axles.Diagnostyka. 2019;20(4):37-48. https://doi.org/10.29354/diag/113001

DIAGNOSTYKA, 2019, Vol. 20, No. 4

ISSN 1641-6414
e-ISSN 2449-5220
DOI: 10.29354/diag/113001

DYNAMIC RESPONSE OF A MULTI-SPAN, ORTHOTROPIC BRIDGE DECK UNDER MOVING TRUCK LOADING WITH TANDEM AXLES

Youcef FISLI [1], Abdelouahab REZAIGUIA [2], Salah GUENFOUD [3], Debra F LAEFER [4]

[1,2,3]Applied Mechanics of New Materials Laboratory, University of 8 May 1945-Guelma, Algeria
[1] tarekfisli@yahoo.fr, [2] rezaiguia.abdelouahab@univ-guelma.dz, [3] strucmec@gmail.com
[4] Center for Urban Science and Progress and Department of Civil Engineering, Tandon School of Engineering
Center for Urban Science and Progress, New York University, United States of America
[4] debra.laefer@nyu.edu

Abstract

In this paper, a new three-dimensional vehicle with tandem axels at the rear is developed to determine dynamic response of bridge deck under load applying truck. The vehicle is modeled by a three-axle dynamic system with 9 degrees of freedom to accurately simulate the disposition and the intensity of loads on the bridge deck. The bridge deck is modeled by a thin, orthotropic, multi-span plate. The road surface irregularities are modeled by a random function characterized by a spectral roughness coefficient and power spectral density. The modal method is used to solve the equation of motion of the bridge deck. Equations of motion of the vehicle are obtained using the virtual work principle. The coupled equations of motion vehicle/bridge deck are integrated numerically by Newmark's method. A computational algorithm in FORTRAN is then elaborated to solve the integrated equations of motion in a decoupled, iterative process. A numerical example of an orthotropic, three-span bridge deck, excited by a 9 degree of freedom truck is presented. The resulting distribution of the Dynamic Amplification Factor (DAF) on the bridge deck does not reflect any particular trend, because high values can be obtained at points where the vertical displacement is small. The DAF is significant only under the interaction force. Thus, the road surface roughness was shown to have a significant influence on the dynamic vehicle/bridge deck interaction forces.

Keywords: dynamic amplification factor; orthotropic bridge deck; vehicle; tandem axles

1. INTRODUCTION

The difference in a structure's response under dynamic loading versus static loading is called its Dynamic Amplification Factor (DAF) and is an especially important phenomenon in the design and analysis of bridges. The DAF caused by vehicles depends on several factors: pavement roughness, singular periodic surface irregularities, wheel irregularities, and each vehicle's mass and speed, as well as the stiffness and damping of the suspension system of the vehicle. The dynamic response of a bridge depends on its span lengths, natural frequencies of vibration, support types, soil structure interaction, physical condition, and viscous damping capabilities [1].

To investigate these issues, Zhu and Law [2] modeled the deck of a multi-span highway bridge by a rectangular orthotropic plate with rigid, intermediate supports. Their vehicle was modeled with a three dimensional (3D) dynamic system with seven degrees of freedom. They studied the influence of the position of the vehicle track on the dynamic response of the bridge and the influence of running speed and road surface irregularities on the bridge's DAF. In related work, Yang et al. [3] studied the extraction of the fundamental frequencies of a bridge from its dynamic response due to the passage of the vehicle; the objective was to comprehend the influence of the vehicle speed on bridge frequencies. They showed in both analytical and finite element studies that the bridge frequency can be extracted from the vehicle acceleration spectrum. Subsequently, Cai et al. [4] developed a fully automatic coupled vehicle/bridge model. The methodology was validated with practical experiments on a typical bridge. The results of the experiments showed that this coupled model reliably predicted the bridge's dynamic response by taking into account the roadway's irregularities. The authors concluded that the initial conditions of the incoming vehicles on the bridge had a significant influence on the dynamic response.

Since then, Yin et al. [5] presented a method to analyze the non-stationary, random response of bridges using the equivalence of a covariance technique. In that, they employed a model of the vehicle with two axles and analyzed three typical bridge models. Numerical results indicated that the non-stationary, random response amplitude of the wheels was proportional to the vehicle speed. They also showed that employing a stationary process to model the disturbance of the roadway profile at different speeds can both underestimate and

overestimate the dynamic effects. In related work, Rezaiguia [6] studied the vibro-acoustic behavior of a multi-span, highway bridge during the passage of vehicle. As part of this, the inclusion of the bridge/vehicle dynamic interaction and random irregularities of the track pavement were investigated.

2. MODELING

In this context, this paper investigates the dynamic behavior of a multi-span bridge deck during a passing truck while incorporating the dynamic vehicle/bridge interaction and the random irregularities of a highway profile. The bridge deck is modeled as an orthotropic, three-span plate. The truck is modeled by a dynamical system with 9 degrees of freedom (DOF) and tandem axles at the rear. The road surface roughness is modeled by a random function characterized by a power spectral density and spectral roughness coefficient. The modal approach is used to solve the equation of motion of the bridge deck. Equations of motion of the vehicle model are obtained by virtual work principle. Numerical integration of coupled equations of the bridge deck and vehicle is performed by the Newmark method, because it is a direct, unconditionally stable method providing maximum precision. Solving these equations is achieved in an uncoupled manner using iterative calculations. Details of this are provided in the following subsections.

2.1. Vehicle model

The vehicle is modeled with a dynamic, lumped-mass-system [7]. The 3D, three axle vehicle with a tandem axle has 9 DOF and consists of a rigid block supported by 6 wheels (Fig. 1). The rigid body representing the truck chassis has 3 DOF (z_{v1} , z_{v2} , z_{v4}) to describe the chassis displacements and rotations. The masses of the axles and wheels are concentrated in lumped masses m_1 to m_6 within the suspension system, leading to a further 6 DOF (z_1 , z_2 , z_3 , z_4 , z_5 , z_6) to describe the vertical wheel displacements. The tire stiffness is modeled using linear springs and viscous dampers.

In Fig. 1, m_i, i = 1, …, 6 are the masses of the wheels with axles of the front and rear axles, m_v, $I_{\theta v}$ and $I_{\alpha v}$ are the mass and moments of inertia of rigid block of the truck, k_{pk} and c_{pk} , k = 1, …, 6 are the tire rigidities and damping respectively, while k_{si} and c_{si} , i = 1, …, 4 are the suspension rigidities and damping, respectively.

In Fig. 2, the forces and moments acting on the vehicle are presented. The equations of motion of the vehicle model are established by applying the virtual work principle, which states that for any cinematically admissible displacement field, the summation of virtual works done by the internal and external forces is zero as per Eq. (1):

$$\delta W = \sum_{i=1}^{4} f_i \delta \Delta_{si} + \sum_{k=1}^{6} \left[F_{pk}^{\text{int}} \delta \Delta_{pk} + m_k \ddot{z}_k \delta z_k + m_k g \delta z_k \right] + \left[m_v \ddot{z}_v \delta z_v + m_v g \delta z_v + m_v \ddot{x}_v \delta x_v + I_{\theta v} \ddot{\theta}_v \delta \theta_v + I_{\alpha v} \ddot{\alpha}_v \delta \alpha_v \right] = 0 \quad (1)$$

where δW is the total virtual work of the vehicle, f_i, F_{pk}^{int} are the forces in the suspensions and in the tires, $\Delta_{si}, \delta \Delta_{pk}$ are the virtual relative displacements of suspensions and tires, $z_k, \delta z_k$ are the displacements and virtual displacements of tires along the vertical axis, $x_v, \delta x_v, z_v, \delta z_v$ are the displacements and virtual displacements of the body of the vehicle along the horizontal and vertical axis, respectively, and $\theta_v, \delta\theta_v, \alpha_v, \delta\alpha_v$ are the rotations and virtual rotations of the rigid block of the vehicle, respectively.

Rotations θ_v, α_v and displacement x_v, z_v are expressed as per Eqs. (2):

$$\theta_v = \frac{z_{v2} - z_{v1}}{s_1}; \ \alpha_v = \frac{z_{v4} - z_{v2}}{s_3};$$
$$x_v = x_1 + \frac{h}{s_1}(z_{v2} - z_{v1}) - a_1 s_1;$$
$$z_v = a_1 z_{v2} + (a_1 - b_2) z_{v2} + b_2 z_{v4} \quad (2)$$

Note that θ_v, α_v are small rotations.

The relative displacements of suspensions Δ_{si} and tires Δ_{pk} are given by Eqs. (3):

$$\Delta_{s1} = z_{v1} - z_1; \ \Delta_{s2} = z_{v2} - (a_4 z_2 + a_3 z_3);$$
$$\Delta_{s3} = z_{v1} - z_{v2} + z_{v4} - z_4;$$
$$\Delta_{s4} = z_{v4} - (a_4 z_5 + a_3 z_6);$$
$$\Delta_{pk} = z_k - w(x_k, y_k, t) - r(x_k, y_k), \ k = 1,...,6 \quad (3)$$

The relative virtual displacements $\delta \Delta_{si}$ and $\delta \Delta_{pk}$ are as shown in Eqs. (4):

$$\delta \Delta_{s1} = \delta z_{v1} - \delta z_1;$$
$$\delta \Delta_{s2} = \delta z_{v2} - (a_4 \delta z_2 + a_3 \delta z_3);$$
$$\delta \Delta_{s4} = \delta z_{v4} - (a_4 \delta z_5 + a_3 \delta z_6);$$
$$\delta \Delta_{pk} = \delta z_k - \delta w - \left(\frac{\partial w}{\partial x} + \frac{\partial r}{\partial x} \right) \delta x_k, \ k = 1,...,6 \quad (4)$$

The suspensions forces of the vehicle are as per Eqs. (5):

$$f_1 = k_{S1}(z_{v1} - z_1) + c_{S1}(\dot{z}_{v1} - \dot{z}_1)$$
$$f_2 = k_{S2}(z_{v2} - a_4 z_2 - a_3 z_3) + c_{S2}(\dot{z}_{v2} - a_4 \dot{z}_2 - a_3 \dot{z}_3)$$
$$f_3 = k_{S3}(z_{v1} - z_{v2} + z_{v4} - z_4) + c_{S3}(\dot{z}_{v1} - \dot{z}_{v2} + \dot{z}_{v4} - \dot{z}_4)$$
$$f_4 = k_{S4}(z_{v4} - a_4 z_5 - a_3 z_6) + c_{S4}(\dot{z}_{v4} - a_4 \dot{z}_5 - a_3 \dot{z}_6) \quad (5)$$

The bridge vehicle interaction forces the in tires are as per Eq. (6)

$$F_{pk}^{\text{int}} = k_{pk}\left[z_k - w(x_k, y_k, t) - r(x_k, y_k)\right] + c_{pk}\left[\dot{z}_k - \frac{\partial w}{\partial t}(x_k, y_k, t) - \left(\frac{\partial w}{\partial x} + \frac{\partial r}{\partial x}\right)_{\substack{x=x_k \\ y=y_k}} \dot{x}_k\right], \; k = 1,..,6 \quad (6)$$

where $w(x_k, y_k, t)$ is the vertical bridge displacement under the kth wheel, $r(x_k, y_k)$ is the road surface roughness under the kth wheel, and z_k is the vertical displacement of the kth wheel.

The equation of the virtual work (1) makes it possible to obtain the equations for each degree of freedom of the model with 9 DOF:

For z_1 :

$$f_1 \delta \Delta_{s1} + F_{p1}^{\text{int}} \delta \Delta_{p1} + m_1 \ddot{z}_1 \delta z_1 + m_1 g \delta z_1 = 0 \quad (7.1)$$

For z_2 :

$$f_2 \delta \Delta_{s2} + F_{p2}^{\text{int}} \delta \Delta_{p2} + m_2 \ddot{z}_2 \delta z_2 + m_2 g \delta z_2 = 0 \quad (7.2)$$

For z_3

$$f_2 \delta \Delta_{s2} + F_{p3}^{\text{int}} \delta \Delta_{p3} + m_3 \ddot{z}_3 \delta z_3 + m_3 g \delta z_3 = 0 \quad (7.3)$$

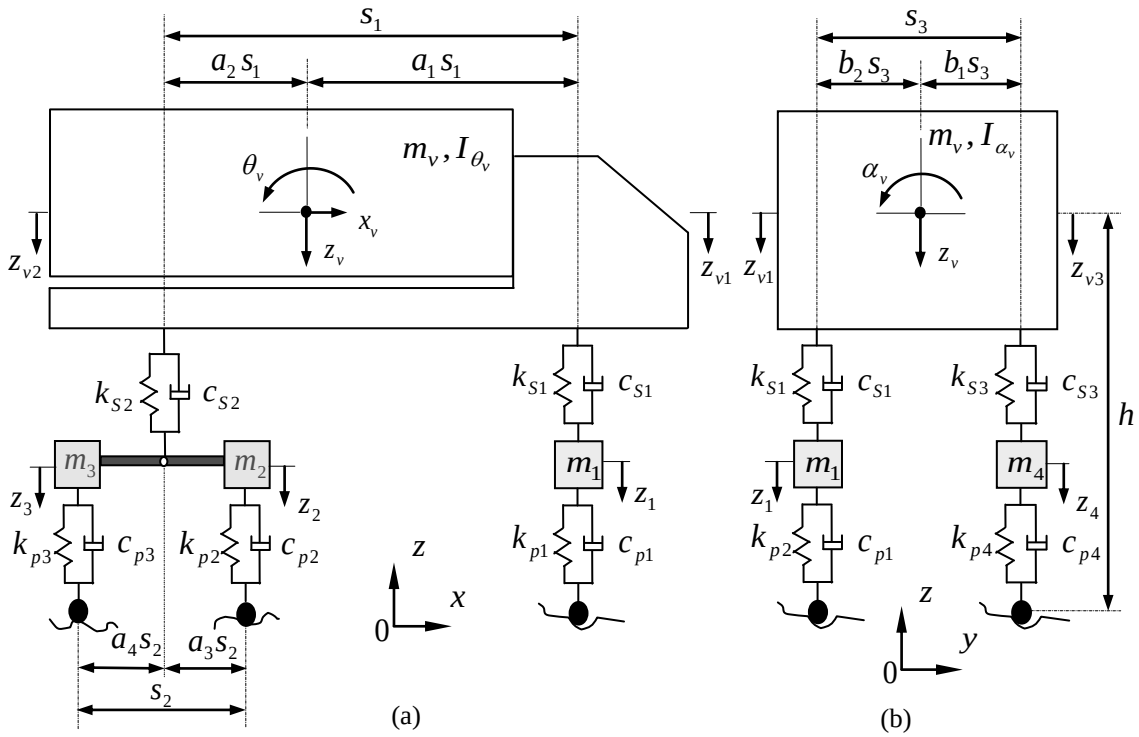

Fig.1. Three axle vehicle model with 9 degrees of freedom, (a): side view, (b): front view

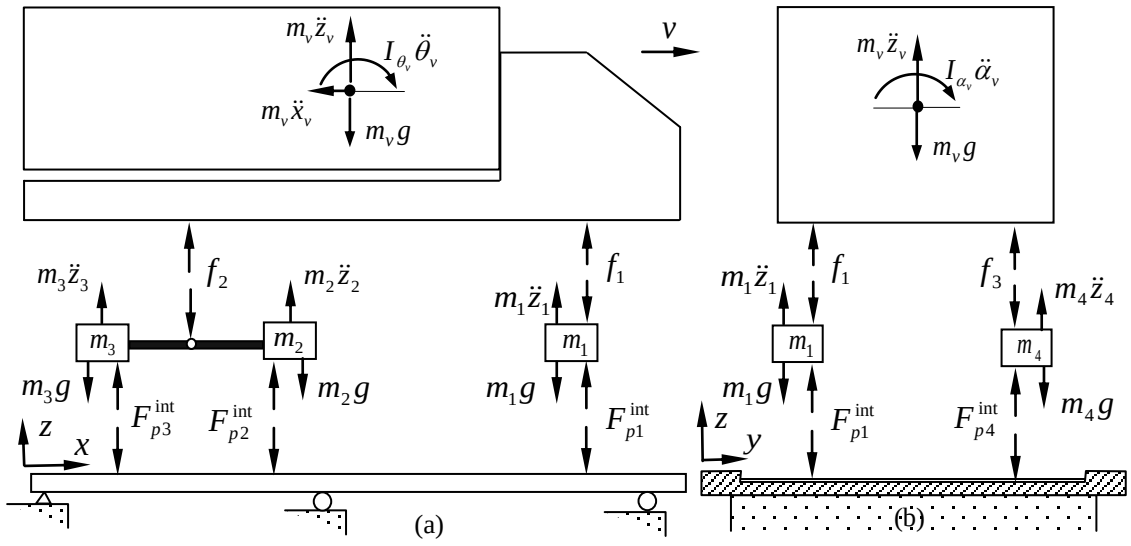

Fig. 2. Dynamic equilibrium of forces and moments, (a): side view, (b): front view

For z_4 :

$$f_3\delta\Delta_{s3} + F_{p4}^{\text{int}}\delta\Delta_{p4} + m_4\ddot{z}_4\delta z_4 + m_4 g\delta z_4 = 0 \quad (7.4)$$

For z_5 :

$$f_4\delta\Delta_{s5} + F_{p5}^{\text{int}}\delta\Delta_{p5} + m_5\ddot{z}_5\delta z_5 + m_5 g\delta z_5 = 0 \quad (7.5)$$

For z_6 :

$$f_4\delta\Delta_{s4} + F_{p6}^{\text{int}}\delta\Delta_{p6} + m_6\ddot{z}_6\delta z_6 + m_6 g\delta z_6 = 0 \quad (7.6)$$

For z_{v1} :

$$f_1\delta\Delta_{s1} + f_3\delta\Delta_{s3} + m_v\ddot{z}_v\delta z_v + m_v g\delta z_v + m_v\ddot{x}_v\delta x_v + I_{\theta v}\ddot{\theta}_v\delta\theta_v = 0 \quad (7.7)$$

For z_{v2} :

$$f_2\delta\Delta_{s2} + f_3\delta\Delta_{s3} + m_v\ddot{z}_v\delta z_v + m_v g\delta z_v + m_v\ddot{x}_v\delta x_v + I_{\theta v}\ddot{\theta}_v\delta\theta_v + I_{\alpha v}\ddot{\alpha}_v\delta\alpha_v = 0 \quad (7.8)$$

For z_{v4} :

$$f_3\delta\Delta_{s3} + f_4\delta\Delta_{s4} + m_v\ddot{z}_v\delta z_v + m_v g\delta z_v + I_{\alpha v}\ddot{\alpha}_v\delta\alpha_v = 0 \quad (7.9)$$

By replacing the various terms of relationships eqs. (2 to 6) in eqs. (7.1)- (7.9) and rejecting the trivial solution for which all the displacements, velocities and accelerations are zero, the system is obtained as per eq. (8):

$$[M_v]\{\ddot{Z}_v\} + [C_v]\{\dot{Z}_v\} + [K_v]\{Z_v\} = \{F_g\} + \{F^{\text{int}}\} \quad (8)$$

where $\{F^{\text{int}}\}$ is the force vector applied to the vehicle, $\{F_g\}$ is the force vector caused by the effect of gravity; $[M_v]$, $[C_v]$ and $[K_v]$ are, respectively, the mass, damping, and stiffness matrices of the vehicle, and $\{Z_v\}$ is the vertical displacement vector of the vehicle's degrees of freedom (see Appendix A).

2.2. Bridge deck model

The bridge deck is modeled as a multi-span, orthotropic, rectangular plate. The bridge is continuous at the intermediate supports, simply supported in $x = 0$ and $x = l$, and free in $y = 0$ and $y = b$ (Fig. 3). The bridge has a linear elastic behavior, and the secondary effects (shearing and inertia of rotation) are neglected. The intermediate supports are linearly rigid and orthogonal at the free edges of the bridge. As the dimensions (length and width) of the bridge deck are much larger than its thickness, thin plate theory is used. The equation of motion of the bridge deck can, therefore, be written as eq. (9):

$$\bar{m}\frac{\partial^2 w}{\partial t^2} + c\frac{\partial w}{\partial t} + D_x\frac{\partial^4 w}{\partial x^4} + 2H\frac{\partial^4 w}{\partial x^2\partial y^2} + D_y\frac{\partial^4 w}{\partial y^4} = -\sum_{k=1}^{nf} F_{pk}^{\text{int}}\delta(x - x_k\ ,\ y - y_k) \quad (9)$$

where $\bar{m} = \rho h$ is the mass density of the plate; c is the viscous damping coefficient of the bridge deck; $D_x = E_x h^3/12(1-\nu_{xy}\nu_{yx})$ and $D_y = E_y h^3/12(1-\nu_{xy}\nu_{yx})$ are flexural rigidities according to x and y directions, respectively; $H = \nu_{xy}D_y + 2D_{xy}$ is the equivalent flexural rigidity; ν_{xy} and ν_{yx} are the Poisson's ratios according to x and y directions respectively; $D_{xy} = G_{xy}h^3/12$ is the torsional rigidity of the bridge deck; G_{xy} is the shear modulus for the xy plane, E_x and E_y are the Young's moduli according x and y directions respectively; F_{pk}^{int} is the interaction force between the k^{th} wheel of the vehicle and the bridge, and (x_k, y_k) is the position of the k^{th} interaction force on the bridge.

Applying the modal superposition method to the bridge deck, the vertical displacement of the orthotropic plate can be written as eq. (10):

$$w(x,y,t) = \sum_{i=1}^{n}\sum_{j=1}^{m}\phi_{ij}(x,y)q_{ij}(t) \quad (10)$$

where $\phi_{ij}(x,y)$ are the mode shapes of a multi-span, continuous, orthotropic plate detailed by Rezaiguia et al. [8], and $q_{ij}(t)$ are the modal coordinates. Substituting eq. (10) into eq. (9), then multiplying by $\phi_{kl}(x,y)$, integrating over the bridge deck surface, and applying the orthogonality conditions of mode shapes, the modal decoupled equations of the system are obtained, as shown in Eq. (11).

$$M_{ij}\ddot{q}_{ij} + C_{ij}\dot{q}_{ij} + K_{ij}q_{ij} = F_{ij} \quad (11)$$

where:

$$M_{ij} = \bar{m}\iint_S \phi_{ij}^{\,2}(x,y)ds \quad (12)$$

$$C_{ij} = c\iint_S \phi_{ij}^{\,2}(x,y)ds = 2\xi_{ij}\omega_{ij}M_{ij} \quad (13)$$

$$K_{ij} = \iint_s\left(D_x\frac{\partial^4\phi_{ij}}{\partial x^4} + 2H\frac{\partial^4\phi_{ij}}{\partial x^2\partial y^2} + D_y\frac{\partial^4\phi_{ij}}{\partial y^4}\right)\phi_{ij}(x,y)dxdy = M_{ij}\omega_{ij}^2 \quad (14)$$

$$F_{ij} = -\iint_s\sum_{k=1}^{nf}F_{pk}^{\text{int}}\delta(x - x_k(t), y - y_k)\ \phi_{ij}(x,y)ds = -\sum_{k=1}^{nf}F_{pk}^{\text{int}}\phi_{ij}(x_k(t), y_k) \quad (15)$$

where M_{ij}, C_{ij}, K_{ij} and F_{ij} are the modal mass, modal damping, modal stiffness and modal forces of the bridge deck, respectively, and ξ_{ij} is the viscous modal damping factors $(\xi_{ij} = c/2\bar{m}\omega_{ij})$.

2.3. Road surface roughness

The road's surface roughness is modeled by a random function characterized by a spectral roughness coefficient and a random variable. There are two approaches to define the characteristics of probabilistic random irregularities of road surface: autocorrelation and spectral density [6]. The static profile of the road surface can be modeled by a stationary Gaussian random process of zero mean

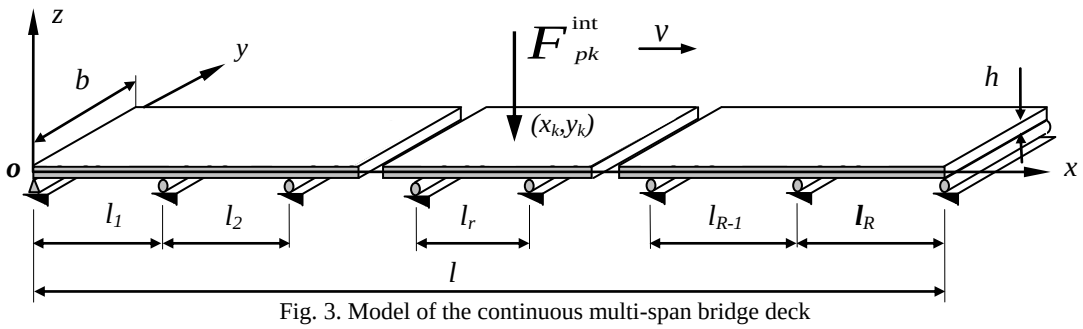

Fig. 3. Model of the continuous multi-span bridge deck

characterized by a Power Spectral Density (PSD), for describing the quality of the running track. The PSD in the frequency domain S_r (depending on the spatial frequency $f_s = \omega_s/2\pi$) associated with this process is given by Eq. (16) as per (Henchi [9], Henchi and al. [10]):

$$s_r(\omega_s) = A_r\left(\frac{\omega_s}{\omega_{s0}}\right)^{-2} \tag{16}$$

where $A_r = A_r(\omega_{s0})$ is the spectral roughness coefficient (value of the spectral density), which characterizes the quality of the running track, and ω_{s0} is the discontinuity angular frequency ($\omega_{s0} = 1/2\pi$).

An approximate representation of a random Gaussian profile can be obtained from a PSD. This representation considers that the profile is the sum of a number of sine waves of random phases θ_i independent and uniformly distributed between 0 and 2π as per Eq. (17):

$$r(x_k) = \sum_{i=1}^{N}\sqrt{4S_r(\omega_{si})\Delta\omega_s}\cos(\omega_{si}x_k + \theta_i) \quad k = 1,2,....,6 \tag{17}$$

where N is the number of discretization points in the frequency domain, ω_{si} is the wave number ($\omega_{si} = 2\pi i/L_c$), $\Delta\omega_s = 2\pi/L_c$, and L_c is typically twice the bridge deck length.

The expression of the discrete value of the PSD is given Eq. (18):

$$s_r(\omega_{si}) = A_r\left(\frac{2\pi\ i}{L_c\omega_{s0}}\right)^{-2} \tag{18}$$

By substituting Eq. (18) into Eq. (17), one obtains Eq. (19):

$$r(x_k) = \sum_{i=1}^{N}\sqrt{4A_r\left(\frac{2\pi i}{L_c\omega_{s0}}\right)\frac{2\pi}{L_c}}\cos(\omega_{si}x_k + \theta_i) \quad k = 1,2,....,6 \tag{19}$$

where x_k is the longitudinal position of the kth vehicle wheel on the bridge deck. This relies on having the length of the roughness wave being greater than the wheel diameter.

2.4. Solving equations of motion

To solve the coupled equations of motion for the bridge deck/vehicle, Newmark's method is applied. eq. (8), which governs the vehicle motion, is written at time $t+\Delta t$ to generate eq. (20):

$$[M_v]\{\ddot{Z}_v\}_{t+\Delta t} + [C_v]\{\dot{Z}_v\}_{t+\Delta t} + [K_v]\{Z_v\}_{t+\Delta t} = \{F_g\} + \{F^{\text{int}}\}_{t+\Delta t} \tag{20}$$

Using Newmark's method, the displacement and velocity respectively are as shown in eq.s (21 and 22):

$$\{Z_v\}_{t+\Delta t} = \{Z_v\}_t + \Delta t\{\dot{Z}_v\}_t + \Delta t^2(0{,}5-\beta)\{\ddot{Z}_v\}_t + \beta\Delta t^2\ \{\ddot{Z}_v\}_{t+\Delta t} \tag{21}$$

$$\{\dot{Z}_v\}_{t+\Delta t} = \{\dot{Z}_v\}_t + (1-\gamma)\Delta t\{\ddot{Z}_v\}_t + \gamma\ \Delta t\{\ddot{Z}_v\}_{t+\Delta t} \tag{22}$$

where γ and β are the stability parameters of Newmark's method, and Δt is the integration time step. By replacing Eq.s (21) and (22) into Eq. (20) and applying factorization one obtain Eq. (23):

$$[S_v]\{\ddot{Z}_v\}_{t+\Delta t} + [C_v]\{\dot{Z}_v^*\}_{t+\Delta t} + [K_v]\{Z_v^*\}_{t+\Delta t} = \{F_g\} + \{F^{\text{int}}\}_{t+\Delta t} \tag{23}$$

with:

$$[S_v] = [M_v] + \gamma\Delta t[C_v] + \beta\ \Delta t^2[K_v] \tag{24}$$

$$\{\dot{Z}_v^*\}_{t+\Delta t} = \{\dot{Z}_v\}_t + (1-\gamma)\Delta t\{\ddot{Z}_v\}_t \tag{25}$$

$$\{Z_v^*\}_{t+\Delta t} = \{Z_v\}_t + \Delta t\{\dot{Z}_v\}_t + (0{,}5-\beta)\Delta t^2\{\ddot{Z}_v\}_t \tag{26}$$

By multiplying Eq. (23) by $[S_v]^{-1}$ one obtains:

$$\{\ddot{Z}_v\}_{t+\Delta t} = \{P_v\}_{t+\Delta t} - [U_v]\{\dot{Z}_v^*\}_{t+\Delta t} - [V_v]\{Z_v^*\}_{t+\Delta t} \tag{27}$$

with:

$$\{P_v\}_{t+\Delta t} = [S_v]^{-1}\left(\{F_g\} + \{F^{\text{int}}\}_{t+\Delta t}\right); \quad [U_v] = [S_v]^{-1}\ [C_v]; [V_v] = [S_v]^{-1}[K_v] \tag{28}$$

Hence, the equation of motion (11) of the bridge deck, at time $t+\Delta t$ can be written as:

$$\ddot{q}_{ij}^{(t+\Delta t)} + 2\xi_{ij}\omega_{ij}\dot{q}_{ij}^{(t+\Delta t)} + \omega_{ij}^2 q_{ij}^{(t+\Delta t)} = \frac{1}{M_{ij}}F_{ij}^{(t+\Delta t)} \tag{29}$$

Using Newmark's method, the generalized displacements and velocities of the bridge deck at time $t+\Delta t$ are, respectively:

$$q_{ij}^{(t+\Delta t)} = q_{ij}^{(t)} + \Delta t\dot{q}_{ij}^{(t)} + \Delta t^2(0{,}5-\beta)\ddot{q}_{ij}^{(t)} + \beta\Delta t^2\ \ddot{q}_{ij}^{(t+\Delta t)} \tag{30}$$

$$\dot{q}_{ij}^{(t+\Delta t)} = \dot{q}_{ij}^{(t)} + (1-\gamma)\Delta t\ddot{q}_{ij}^{(t)} + \gamma\ \Delta t\ddot{q}_{ij}^{(t+\Delta t)} \tag{31}$$

By substituting expressions (30) and (31) into Eq. (29), one obtains:

$$\ddot{q}_{ij}^{(t+\Delta t)} = \frac{\left(\frac{1}{M_{ij}}F_{ij}^{(t+\Delta t)} - 2\xi_{ij}\omega_{ij}\dot{q}_{ij}^{*(t+\Delta t)} - \omega_{ij}^2 q_{ij}^{*(t+\Delta t)}\right)}{\left(1 + 2\Delta t\xi_{ij}\omega_{ij} + \beta\Delta t^2\omega_{ij}^2\right)} \tag{32}$$

with:

$$q_{ij}^{*(t+\Delta t)} = q_{ij}^{(t)} + \Delta t\dot{q}_{ij}^{(t)} + (0{,}5-\beta)\Delta t^2\ddot{q}_{ij}^{(t)} \tag{33}$$

$$\dot{q}_{ij}^{*(t+\Delta t)} = \dot{q}_{ij}^{(t)} + (1-\gamma)\Delta t\ddot{q}_{ij}^{(t)} \tag{34}$$

2.5. Solution algorithm

The algorithm of resolution contains two loops (Fig. 4). The first corresponds to the time and the second to the iterations. Displacements, speeds, and accelerations of the bridge deck and vehicle are approximated from the previous iteration $(\bar{k})$, and then one calculates the interaction forces at each contact point. From there, one solves the vehicle equation of motion Eq. (20) by using Newmark's method. Then one calculates the vector of interaction forces acting on the bridge deck at each contact point. One can solve the modal Eq. (29) for the bridge deck by Newmark's method. One then makes a convergence test between the displacement $w^{(\bar{k}+1)}$ of the iteration $(\bar{k}+1)$ and the displacement $w^{(\bar{k})}$ of the previous iteration as follows:

$$\left|w^{(\bar{k}+1)}(x,y,t)-w^{(\bar{k})}(x,y,t)\right| \le \varepsilon \tag{35}$$

If this condition is satisfied, the desired dynamic parameters can then be calculated. One then proceeds to the next time step. If, however, if the condition (35) is not verified, one must apply a correction during the next iteration so that the displacement $w^{(\bar{k}+1)}$ becomes an approximation of the subsequent iteration. One then recalculates, until convergence is achieved.

- Read data for the bridge deck
- Read data for the vehicle model
- Read data for the pavement

- Calculate: $D_x, D_y, H, D_{xy}, G_{xy}, \overline{m}$
- Select the number of modes and calculate frequencies and mode shapes: ω_{ij}, ϕ_{ij}
- Select the traveling speed: v
- Select the time step Δt, parameters γ, β and the tolerance ε
- Calculate modal masses, stiffnesses and dampings of the bridge deck: M_{ij}, K_{ij}, C_{ij}
- Calculate the matrices mass, stiffness and damping of the vehicle model: $[M_v], [C_v], [K_v]$
- Select the initial conditions: $\{q\}_0, \{\dot{q}\}_0, \{\ddot{q}\}_0, \{Z_v\}_0, \{\dot{Z}_v\}_0, \{\ddot{Z}_v\}_0$
- Determine transverse wheel positions: y_k

For each time step $t = t + \Delta t$ **:**

- Determine the longitudinal position of vehicle on the bridge deck: $x_k = v\ t_k$
- Calculate in each contact point *k*: $r(x_k), r'(x_k)$
- Approximate the displacements, speeds, and accelerations of the bridge deck and vehicle from the previous iteration

For each iteration: $\bar{k} = \bar{k} + 1$

- Calculate at each contact point k : $w(x_k), \dot{w}(x_k), \dot{r}(x_k)$
- Calculate the interaction forces $F_k^{\text{int}} = k_{pk}(w_k + r_k) + c_{pk}(\dot{w}_k + \dot{r}_k)$
- Calculate the vector $\{F^{\text{int}}\}$
- Calculate the forces vector related the gravity effects: $\{F_g\}$
- Solve with Newmark's method: $[M_v]\{\ddot{Z}_v\} + [C_v]\{\dot{Z}_v\} + [K_v]\{Z_v\} = \{F_g\} + \{F^{\text{int}}\}$
- Calculate the interaction forces acting on the bridge deck at each contact point: $F_{pk}^{\text{int}} = k_{pk}(w_k + r_k - z_k) + c_{pk}(\dot{w}_k + \dot{r}_k - \dot{z}_k)$
- Solve with Newmark's method: $\ddot{q}_{ij} + 2\xi_{ij}\omega_{ij}\dot{q}_{ij} + \omega_{ij}^2 q_{ij} = \dfrac{1}{M_{ij}} F_{ij}$
- Calculate the vertical displacement of the bridge deck: $w^{(\bar{k}+1)}(x,y,t) = \sum_{i=1}^{n}\sum_{j=1}^{m} \phi_{ij}(x,y) q^{(\bar{k}+1)}{}_{ij}(t)$
- Convergence test:

  If no $\left|\omega^{(\bar{k}+1)}(x,y,t) - \omega^{(\bar{k})}(x,y,t)\right| \le \varepsilon$ if yes so

- Calculate the dynamic parameters desired.

Fig. 4. The computational algorithm for the decoupled method

3. NUMERICAL EXAMPLE

In this example, the dynamic behavior of a deck slab bridge is modeled by a three-span orthotropic rectangular plate was excited with a moving vehicle modeled by a dynamic model with 9 DOF. The equivalent properties of the deck slab are as per [6]: l = 78 *m*, $l_1 = l_3$ = 24 *m* and l_2 = 30 *m*, b = 13.715 *m*, h = 0.212 *m*, ρ = 3265 kg/m^3, D_x= 2.41 × 10^9 *Nm*, D_y = 2.18 × 10^7 *Nm*, D_{xy} = 1.14 × 10^8 *Nm*, ν_{xy} = 0.3, E_x = 3.06 × 10^{12} *N*/m^2, E_y= 2.76 × 10^{10} *N*/m^2, G_{xy} = 1.45 × 10^{11} *N*/m^2. The natural frequencies and mode shapes of the three-span orthotropic bridge deck were calculated with a recently developed approach based on the modal method incorporating the effect of intermodal coupling neglected in previous similar studies. The first 10 natural frequencies in Hz, of the deck slab were as reported in [11]: 4.13, 5.45, 6.30, 7.59, 7.75, 9.77, 9.08, 11.26, 11.97, and 15.07. Figure 5 shows the geometry and mass distribution of the vehicle considered for this study, the details of the vehicle are from [7] and summarized in Table 1.

Table 2 presents the experimental values of the spectral roughness coefficient *Ar* according to the state of the track [9]. Based on the expression (19) of the road profile, Fig. 6 shows the random profile of the track for different values of the spectral coefficient roughness.

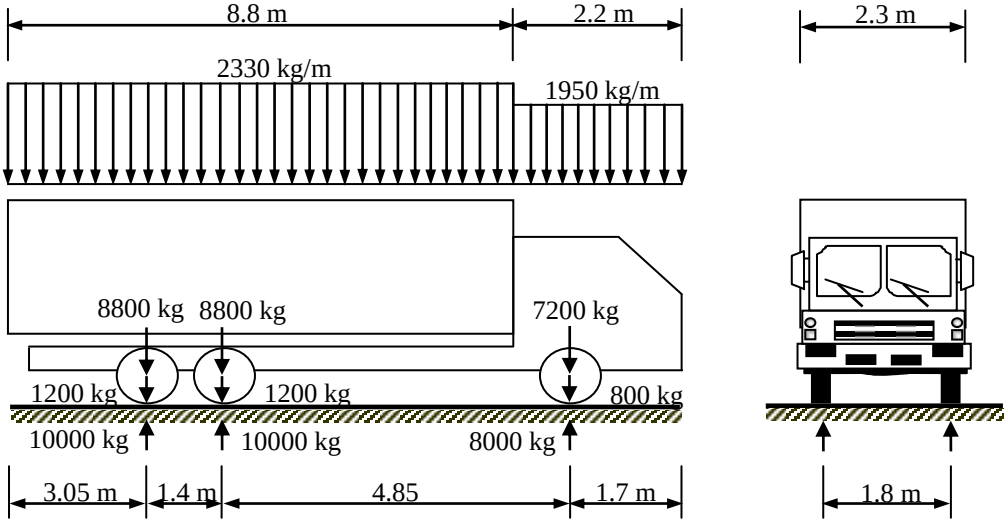

Fig. 5. Geometry and mass distribution of the truck

Table 1. Vehicle parameters [7]

Geometry	Height of gravity center of the vehicle	h = 1.8 m
	Spacing between front axle and tandem	s_1 = 5.55 m
	Spacing between vehicle tires	s_3 = 1.8 m
	Eccentricities	a_1 = 0.71, a_2 = 0.29, $a_3 = a_4$ = 0.5, $b_1 = b_2$ = 0.5
Masses	Rigid block of the vehicle	m_v = 24800 kg
	front wheels	$m_1 = m_4$ = 800 kg
	wheels of the first rear axle	$m_2 = m_5$ = 1200 kg
	wheels of the second rear axle	$m_3 = m_6$ = 1200 kg
Moments of inertia	Rigid block of the vehicle (pitch)	$I_{\theta v}$ = 241359 kg m^2
	Rigid block of the vehicle (roll)	$I_{\alpha v}$ = 34878.468 kg m^2
Stiffnesses	Front suspensions	$k_{s1} = k_{s3}$ = 520000 N/m
	Rear suspensions	$k_{s2} = k_{s4}$ = 2348000 N/m
	Front tires	$k_{p1} = k_{p4}$ = 2000000 N/m
	Tires of the first rear axle	$k_{p2} = k_{p5}$ = 4000000 N/m
	Tires on the second rear axle	$k_{p3} = k_{p6}$ = 4000000 N/m
Dampings	Front suspensions	$c_{s1} = c_{s3}$ = 12194 N s/m
	Rear suspensions	$c_{s2} = c_{s4}$ = 40715 N s/m
	Front tires	$c_{p1} = c_{p4}$ = 4000 N s/m
	tires of the first rear axle	$c_{p2} = c_{p5}$ = 6928 N s/m
	Tires on the second rear axle	$c_{p3} = c_{p6}$ = 6928 N s/m

Table 2. Experimental values of A_r according to the type of the track [9]

Track conditions	Very good	good	moderate	Bad
A_r (m^3/cycle) ×10^{-6}	A_r < 5	5< A_r < 20	20< A_r < 80	80< A_r < 256

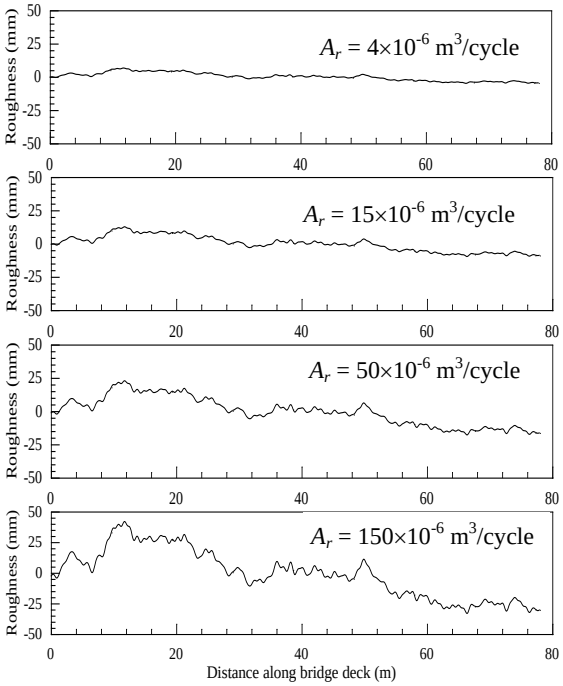

Fig. 6. Random profile of the track for different values of roughness coefficient A_r

3.1 Influence of the loading mode

Several numerical simulations were performed to identify the influence of the moving load on the dynamic responses of the deck slab bridge. The truck traversed the bridge at a speed of 100 km/h along three different paths (Fig. 7). Before calculating the dynamic response of the bridge deck, we checked its convergence with multiple numbers of modes. The results demonstrated that 10 modes are sufficient for the convergence of the modal series (9). In the results section, we chose i = 1, ..., 9 and j = 1, ..., 5 so 45 modes, which are more than enough for the convergence. The vertical displacement of the bridge deck must be corrected at all six contact points to obtain the dynamic equilibrium between the bridge deck and vehicle at each time step. The iterative process is detailed in section 2.5. The iterative process usually converges in two to four iterations in each time step.

Table 3 and figures 8 shows the influence the influence of the loading mode on the DAF calculated in the middle of each span and in the middle of each girder. The maximum static response is obtained with the truck moving at the very slow speed of 0.01m/s. Based on those conditions, the following was observed

- The DAF is small near the vehicle and higher further away.
- The DAF of the middle of girders 4 and 5 were the highest for the first and second loading cases (DAF = 2.63 and 2.19). This may be due either to torsional modes excited by these loading cases or with the definition itself of the dynamic amplification factor as a response indicator.

Fig. 9 illustrates the influence of the loading mode on the vertical displacement at the middle point of a three-span bridge deck. This image shows the following

- High vertical displacement near the applied load, while the DAF is the opposite (see Table 3 and Fig.9).
- Positive vertical displacement when the load is eccentric (i.e. when the truck is located on either the first or the third span).

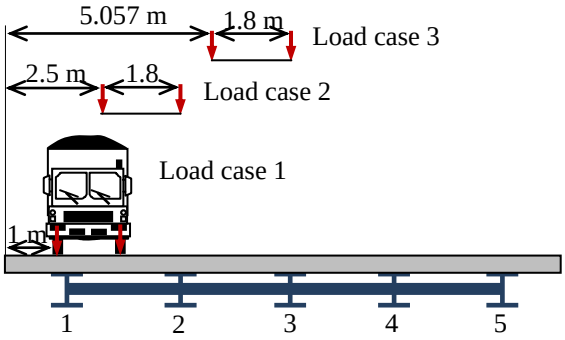

Fig. 7. Vehicle loading

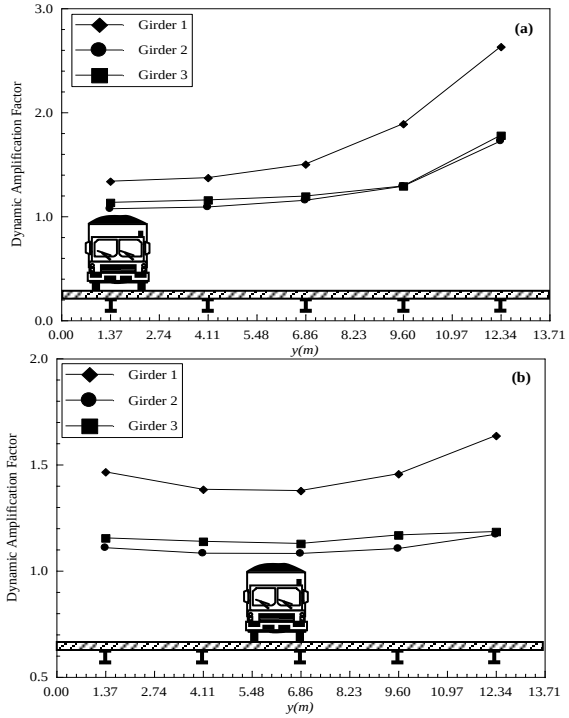

Fig. 8. Distribution of the Dynamic Amplification Factor in the cross section of the bridge deck, (a): load case 1, (b): load case 3

Table 3. Distribution of the dynamic amplification factor on the bridge deck

Load case	Span	Dynamic Amplification Factor				
		Girder 1	Girder 2	Girder 3	Girder 4	Girder 5
1	1	1.337	1.371	1.501	1.889	2.630
	2	1.072	1.089	1.153	1.288	1.723
	3	1.133	1.157	1.194	1.291	1.778
2	1	1.333	1.360	1.435	1.695	2.191
	2	1.072	1.087	1.101	1.199	1.364
	3	1.137	1.135	1.171	1.224	1.402
3	1	1.465	1.383	1.377	1.456	1.636
	2	1.108	1.082	1.081	1.104	1.171
	3	1.154	1.138	1.128	1.168	1.184

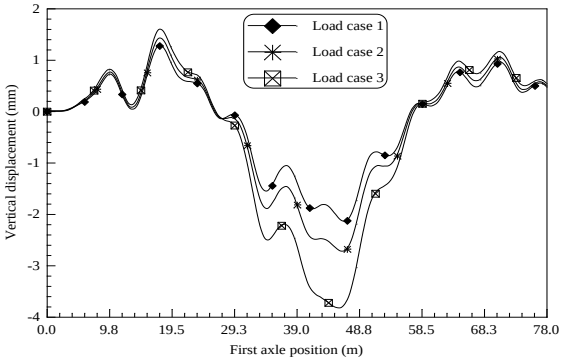

Fig. 9. Vertical displacement at middle of span 2 of girder 3 under different loadings

3.2. Influence of vehicle speed

Fig. 10 shows the influence of the vehicle speed on the vertical displacement in the middle of the bridge deck (span 2, girder 3). The truck through the bridge deck according to loading case 1. For a very low speed, the vertical displacement in the middle of the bridge deck tends to the static vertical displacement. The maximum of the vertical displacement in the middle of the bridge deck increases as the vehicle speeds up to 133.2 km/h then decreases and it shifts upwards in the rolling direction of the vehicle.

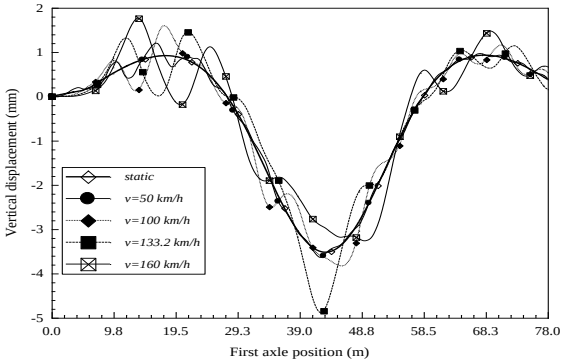

Fig. 10. Influence of the vehicle speed on the vertical displacement of the middle

Fig. 11 shows the variation of the dynamic amplification factor of the bridge deck at the middle point girder 1 and 3 and in the middle of the span 2, under different loading cases as a function of the vehicle speed selected between 10 and 160 km/h. The DAF varies little up to vehicle speeds of around 110 km/h. After which, a rapid increase occurs at a critical speed of 133.2 km/h followed by a rapid decline

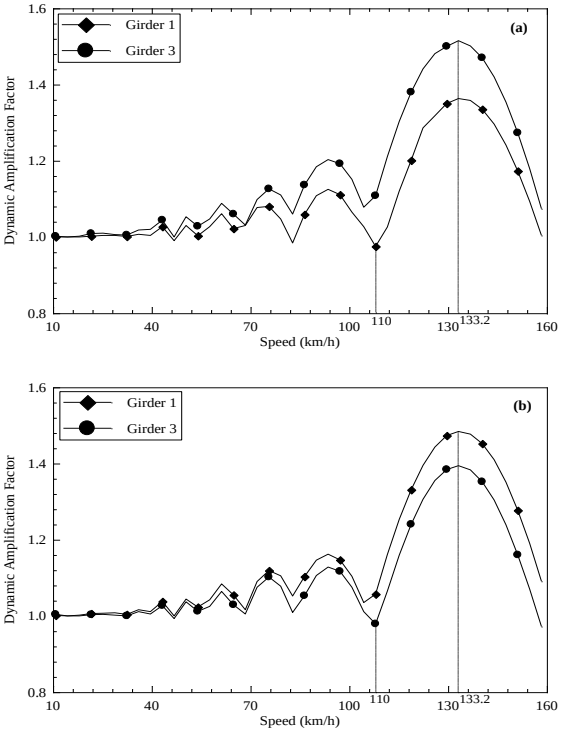

Fig. 11. Dynamic amplification factor at middle of span 2 of girders 1 and 3 as function of vehicle speed, (a): load case 1, (b): load case 3

3.3. Influence of vehicle mass

The mass difference between the loaded and unloaded truck can cause changes in the dynamic behavior of the bridge deck. To identify the influence of the truck mass on the dynamic response of the bridge deck, three load levels were simulated for the truck: an unloaded truck (m_v = 8200 kg), a normally loaded truck (m_v = 24800 kg), and an overloaded truck (m_v = 31300 kg). Fig.12 shows the influence of the vehicle mass on the vertical displacement in the middle of the bridge deck. The truck through the bridge according to

path of the load case 3 at a speed of 80 km/h. As expected, there is an increase of the vertical displacement in the middle of the bridge deck, especially when the truck is overloaded and located within the central span.

Fig.13 shows the influence of the truck mass on the dynamic amplification factor in the middle of girder 3 and the middle of span 2 with truck speeds from 10 to 160 km/h. Those results demonstrated the following:

- The critical speed corresponding to the maximum dynamic amplification factor decreases with the truck mass: for the unloaded truck the critical speed was 144 km/h, for the normally loaded truck 133.2 km/h, and for the overloaded truck 126 km/h demonstrating the relationship between a decreasing critical speed with an increasing vehicle weight.
- For the critical speed, the DAF was higher in the case of the normally loaded truck

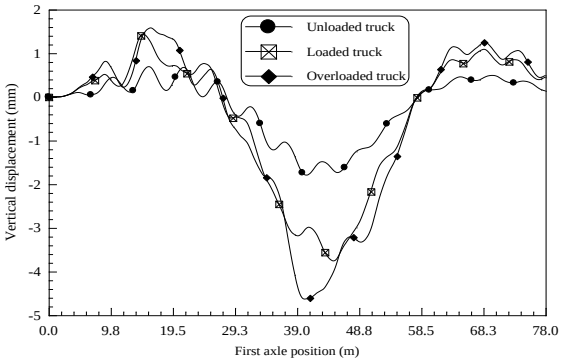

Fig. 12. Vertical displacement at middle of span 2 of girder 3 under different mass vehicle, v_x = 80 km/h, load case 3

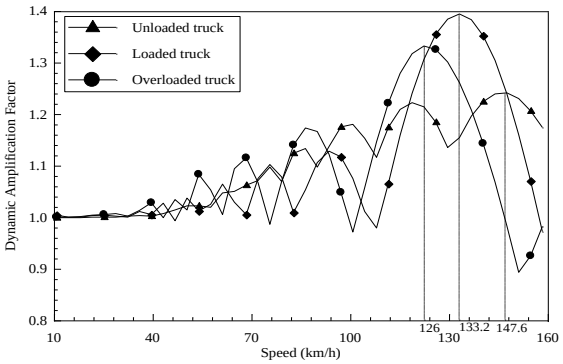

Fig. 13. Influence of vehicle mass on DAF in the middle of the bridge deck

3.4. Influence of road surface roughness

Fig.14 shows the influence of the road surface roughness on the DAF in the middle of span 2, girder 3, for vehicle speeds varying from 10 to 160 km/h. The vehicle passes along the bridge deck under loading case 3. Notably, increased road surface roughness increases the DAF in the tread slab. Additionally, at a speed of 133.2 km/h and a bad road surface (A_r = 150 × 10^{-6} m^3/cycle), an increase of about 25 % of the maximum value of the DAF occurred.

Fig.15 shows the variation of the interaction forces exerted by a right rear wheel of the vehicle based on the track conditions. The vehicle was moving at a speed of 100 km/h according to load case 3. The results showed that changes in the amplitudes of the interaction forces increased significantly with greater track profile roughness. This means that the state of the track can more significantly influence the vehicle vibrations than the rolling slab. Additionally, the interaction forces fluctuated around an average value, which corresponded to the static force.

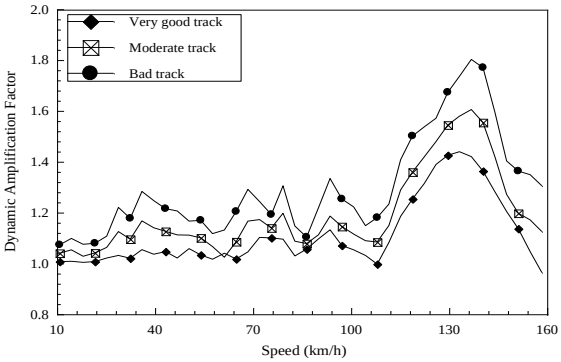

Fig. 14. Influence of the state of the track on the dynamic amplification factor in the middle of the deck slab for loading case 3

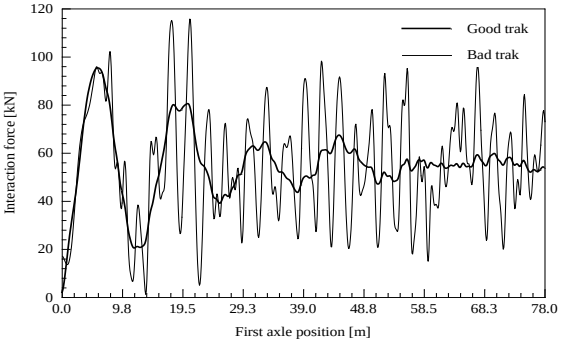

Fig. 15. Interaction force exerted by a right rear wheel of the vehicle, v_x=100 km/h,

4. CONCLUSIONS

In this paper, the dynamic interaction between a moving vehicle (modeled as a 9 DOF dynamic system with tandem axles) and a bridge (modeled as a three-span orthotropic plate) was studied taking into account road surface irregularities. The modal method and Newmark's numerical integration were used to solve the coupled equations of bridge/vehicle motion. For this, an iterative algorithm was proposed for solving the coupled equations of bridge/vehicle motion in a decoupled manner. Numerical simulations were performed to study the variation of dynamic amplification factor on the bridge deck. Three major observations were made:

- High dynamic amplification factors can occur in places where the vertical displacement is small.

- In the case studied, the critical speed corresponding to the maximum dynamic amplification factor was about 133.2 km/h. This value varies according to the vehicle mass.
- The effect of track irregularities on the dynamic response of the bridge deck and interaction forces is the most important parameter.

APPENDIX A

The equations of motion of the vehicle model with 9 degrees of freedom are given by:

$$[M_v]\{\ddot{Z}_v\}+[C_v]\{\dot{Z}_v\}+[K_v]\{Z_v\}=\{F_g\}+\{F^{\text{int}}\}$$

with:

$$\{Z_v\}=\{z_1,z_2,z_3,z_4,z_5,z_6,z_{v1},z_{v2},z_{v4}\}^T$$

The matrices $[M_v]$, $[C_v]$ and $[K_v]$ are symmetrical. Element of matrix $[M_v]$ are as flows:

$$m_{v11}=m_1$$

$$m_{v22}=m_2;\ m_{v23}=m_{v24}=m_{v25}=m_{v26}=m_{v27}=m_{v28}=m_{v29}=0;$$

$$m_{v33}=m_3;\ m_{v34}=m_{v35}=m_{v36}=m_{v37}=m_{v38}=m_{v39}=0;$$

$$m_{v44}=m_4;\ m_{v45}=m_{v46}=m_{v47}=m_{v48}=m_{v49}=0;$$

$$m_{v55}=m_5;\ m_{v56}=m_{v57}=m_{v58}=m_{v59}=0;$$

$$m_{v66}=m_6;\ m_{v67}=m_{v68}=m_{v69}=0;$$

$$m_{v77}=m_v\left(a_2^2+\frac{h^2}{s_1^2}\right)+\frac{I_{\theta v}}{s_1^2};\ m_{v78}=m_v\left[a_1a_2-a_2b_2-\frac{h^2}{s_1^2}\right]-\frac{I_{\theta v}}{s_1^2};$$

$$m_{v79}=m_va_2b_2;$$

$$m_{v88}=m_v\left[(a_1-b_2)^2+\frac{h^2}{s_1^2}\right]+\frac{I_{\theta v}}{s_1^2}+\frac{I_{\alpha v}}{s_3^2};$$

$$m_{v89}=m_v\left[a_1b_2-b_2^2\right]-\frac{I_{\alpha v}}{s_3^2}$$

$$m_{v99}=m_vb_2^2+\frac{I_{\alpha v}}{s_3^2};$$

Element of matrix $[C_v]$ are as flows:

$$c_{v11}=c_{s1}+c_{p1};\ c_{v17}=-c_{s1};$$

$$c_{v12}=c_{v13}=c_{v14}=c_{v15}=c_{v16}=c_{v18}=c_{v19}=0;$$

$$c_{v22}=c_{s2}a_3^2+c_{p3};\ c_{v23}=-c_{s2}a_3a_4;$$

$$c_{v28}=-c_{s2}a_4;$$

$$c_{v24}=c_{v25}=c_{v26}=c_{v27}=c_{v29}=0;$$

$$c_{v33}=c_{s2}a_3^2+c_{p3};\ c_{v38}=-c_{s2}a_3;$$

$$c_{v34}=c_{v35}=c_{v36}=c_{v37}=c_{v39}=0;$$

$$c_{v44}=c_{s3}+c_{p4};\ c_{v45}=c_{v46}=0;\ c_{v47}=-c_{s3};$$

$$c_{v48}=c_{s3};\ c_{v49}=-c_{s3};$$

$$c_{v55}=c_{s4}a_4^2+c_{p5};\ c_{v56}=c_{s4}a_4^2+c_{p5};$$

$$c_{v57}=c_{v58}=0;\ c_{v59}=-c_{s4}a_4;$$

$$c_{v66}=c_{s4}a_3^2+c_{p6};\ c_{v67}=c_{v68}=0;$$

$$c_{v69}=-c_{s4}a_3;$$

$$c_{v77}=c_{s1}+c_{s3};\ c_{v78}=-c_{s3};\ c_{v79}=c_{s3};$$

$$c_{v88}=c_{s2}+c_{s3};\ c_{v89}=-c_{s3};\ c_{v99}=c_{s3}+c_{s4};$$

Elements of the $[K_v]$ matrix are similar to elements of $[C_v]$ matrix, by replacing the damping c_{sk} by rigidities k_{sk}

Element of vector $\{F^{\text{int}}\}$ are as flows:

$$\{F^{\text{int}}\}=\begin{Bmatrix}
k_{p1}[w(x_1,y_1,t)+r(x_1,y_1)]+c_{p1}\left[\frac{\partial w}{\partial t}(x_1,y_1,t)+\left(\frac{\partial w}{\partial x}+\frac{\partial r}{\partial x}\right)_{x=x_1,y=y_1}\dot{x}_1\right]\\
k_{p2}[w(x_2,y_2,t)+r(x_2,y_2)]+c_{p2}\left[\frac{\partial w}{\partial t}(x_2,y_2,t)+\left(\frac{\partial w}{\partial x}+\frac{\partial r}{\partial x}\right)_{x=x_2,y=y_2}\dot{x}_1\right]\\
k_{p3}[w(x_3,y_3,t)+r(x_3,y_3)]+c_{p3}\left[\frac{\partial w}{\partial t}(x_3,y_3,t)+\left(\frac{\partial w}{\partial x}+\frac{\partial r}{\partial x}\right)_{x=x_3,y=y_3}\dot{x}_1\right]\\
k_{p4}[w(x_4,y_4,t)+r(x_4,y_4)]+c_{p4}\left[\frac{\partial w}{\partial t}(x_4,y_4,t)+\left(\frac{\partial w}{\partial x}+\frac{\partial r}{\partial x}\right)_{x=x_4,y=y_4}\dot{x}_1\right]\\
k_{p5}[w(x_5,y_5,t)+r(x_5,y_5)]+c_{p5}\left[\frac{\partial w}{\partial t}(x_5,y_5,t)+\left(\frac{\partial w}{\partial x}+\frac{\partial r}{\partial x}\right)_{x=x_5,y=y_5}\dot{x}_1\right]\\
k_{p6}[w(x_6,y_6,t)+r(x_6,y_6)]+c_{p6}\left[\frac{\partial w}{\partial t}(x_6,y_6,t)+\left(\frac{\partial w}{\partial x}+\frac{\partial r}{\partial x}\right)_{x=x_6,y=y_6}\dot{x}_1\right]\\
0\\0\\0
\end{Bmatrix}$$

Element of vector $\{F_g\}$ are as flows:

$$\{F_g\}=\left\{-m_1g,-m_2g,-m_3g,-m_4g,-m_5g,-m_6g,-a_2m_vg+m_v\frac{h}{s_1}\ddot{x}_1,\right.$$
$$\left.-(a_1-b_2)m_vg-m_v\frac{h}{s_1}\ddot{x}_1,-b_2m_vg\right\}^T$$

5. REFERENCES

1. Isabel GT. Analyse par éléments finis de l'interaction dynamique entre les trains et les ponts ferroviaires. Mémoire de Maître ès en Art, Université Laval, Canada, 2001.
2. Zhu XQ, Law SS. Dynamic load on multi-lane bridge deck from moving vehicles. Journal of Sound and Vibration 2002; 251: 697-716. https://doi.org/10.1006/jsvi.2001.3996
3. Yang YB, Lin CW, Yau JD. Extracting bridge frequencies from the dynamic response of a passing vehicle. Journal of Sound and Vibration 2004; 272: 471-493. https://doi.org/10.1016/S0022-460X(03)00378-X
4. Cai CS, Shi XM, Araujo M, Chen SR. Effect of approach span condition on vehicle-induced dynamic response of slab-on-girder road bridges. Engineering Structures 2007; 29: 3210–3226. https://doi.org/10.1016/j.engstruct.2007.10.004
5. Yin X, Fang Z, Cai CS, Deng L. Non-stationary random vibration of bridges under vehicles with variable speed. Engineering Structures 2010; 32: 2166-2174. https://doi.org/10.1016/j.engstruct.2010.03.019
6. Rezaiguia A. Vibroacoustic modelling of highway bridges crossing by moving vehicles. Doctorate Thesis, Annaba University, Algeria, 2008.

7. Broquet C. Comportement des dalles de roulement des routes en béton sollicitées par le trafic routier. Thèse PhD., Ecole Polytechnique Fédéral, Lausanne, 1999.
8. Rezaiguia A**,** Fisli Y, Ellagoune S**,** Laefer DF, Ouelaa N. Extension of semi- analytical approach to determine natural frequencies and mode shapes of a multi-span orthotropic bridge deck. Structural Engineering and Mechanics 2012; 43: 71-87. http://dx.doi.org/10.12989/sem.2012.43.1.071
9. Henchi K. Dynamic analysis of bridges by finite elements method under mobile vehicles solicitation. PhD Thesis, Compiegne University of Technology, French, 1995.
10. Henchi K, Fafard M, Talbot M, Dhatt G. An efficient algorithm for dynamic analysis of bridges under moving vehicles using a coupled modal and physical components approach. Journal of Sound and Vibration 1998; 212: 663-683. https://doi.org/10.1006/jsvi.1997.1459
11. Rezaiguia A, Laefer DF. Semi-analytical determination of natural frequencies and mode shapes of multi-span bridge decks. Journal of Sound and Vibration 2009; 328: 291-300. https://doi.org/10.1016/j.jsv.2009.08.007

Received 2019.06.09
Accepted 2019.20.12
Available online 2019-10-14

Youcef FISLI, received his Magister degree in Mechanical Engineering in 2011 from University of 8 may 1945-Guelma, Algeria. He is a PhD student in Applied Mechanics of New Materials Laboratory at the same University. Areas of interest: structures, vibrations and modeling.

Abdelouahab REZAIGUIA, received his PhD degree in Mechanical Engineering in 2008 from Annaba University and his Habilitation in 2013 from University of 8 may 1945-Guelma, Algeria. He is a member of Applied Mechanics of New Materials Laboratory. He works at the Department of Mechanical Engineering at the same University. Research topics: Dynamic behavior of structures under moving loads, Rotordynamics.

Debra LAEFR, received her PhD degree in civil engineering in 2001 from the University of Illinois Urbana-Champaign. She is a Full Professor in the Department of Civil and Urban Engineering at New York University and leads the Urban Modeling Group at the Center for Urban Science and Progress.

Salah GUENFOUD, received his PhD degree in Structural Mechanics in 2001 from the Belarusian National Technical University. He is a Professor in the Department of Mechanical Engineering in 8 may 1945 University-Guelma, Algeria. He is a member of Applied Mechanics of New Materials Laboratory. Research topics: modeling of the structures with any boundary conditions in static and dynamic, modeling of structures of composite materials, inverse problems.